

RESEARCH ARTICLE | SEPTEMBER 08 2020

Effect of reactant dosing on selectivity during area-selective deposition of TiO₂ via integrated atomic layer deposition and atomic layer etching

Holger Saare ; Seung Keun Song ; Jung-Sik Kim ; Gregory N. Parsons  



J. Appl. Phys. 128, 105302 (2020)

<https://doi.org/10.1063/5.0013552>



Articles You May Be Interested In

In situ studies on atomic layer etching of aluminum oxide using sequential reactions with trimethylaluminum and hydrogen fluoride

J. Vac. Sci. Technol. A (April 2022)

Comparison of BCl₃, TiCl₄, and SOCl₂ chlorinating agents for atomic layer etching of TiO₂ and ZrO₂ using tungsten hexafluoride

J. Vac. Sci. Technol. A (June 2023)

Atomic layer deposition of Ta-based thin films: Reactions of alkylamide precursor with various reactants

J. Vac. Sci. Technol. B (September 2006)

Effect of reactant dosing on selectivity during area-selective deposition of TiO₂ via integrated atomic layer deposition and atomic layer etching

Cite as: J. Appl. Phys. 128, 105302 (2020); doi: 10.1063/5.0013552

Submitted: 12 May 2020 · Accepted: 25 August 2020 ·

Published Online: 8 September 2020



View Online



Export Citation



CrossMark

Holger Saare,¹ Seung Keun Song,² Jung-Sik Kim,² and Gregory N. Parsons^{1,2,a)}

AFFILIATIONS

¹ Department of Physics, North Carolina State University, Raleigh, North Carolina 27695, USA

² Department of Chemical and Biomolecular Engineering, North Carolina State University, Raleigh, North Carolina 27695, USA

^{a)}Author to whom correspondence should be addressed: gnp@ncsu.edu

ABSTRACT

A key hallmark of atomic layer deposition (ALD) is that it proceeds via self-limiting reactions. For a good ALD process, long reactant exposure times beyond that required for saturation on planar substrates can be useful, for example, to achieve conformal growth on high aspect ratio nanoscale trenches, while maintaining consistent deposition across large-area surfaces. Area-selective deposition (ASD) is becoming an enabling process for nanoscale pattern modification on advanced nanoelectronic devices. Herein, we demonstrate that during area-selective ALD, achieved by direct coupling of ALD and thermal atomic layer etching (ALE), excess reactant exposure can have a substantially detrimental influence on the extent of selectivity. As an example system, we study ASD of TiO₂ on hydroxylated SiO₂ (Si-OH) vs hydrogen-terminated (100) Si (Si-H) using TiCl₄/H₂O for ALD and WF₆/BCl₃ for ALE. Using *in situ* spectroscopic ellipsometry and *ex situ* x-ray photoelectron spectroscopy, we show that unwanted nucleation can be minimized by limiting the water exposure during the ALD steps. Longer exposures markedly increased the rate of nucleation and growth on the desired non-growth region, thereby degrading selectivity. Specifically, transmission electron microscopy analysis demonstrated that near-saturated H₂O doses enabled 32.7 nm thick TiO₂ patterns at selectivity threshold S > 0.9 on patterned Si/SiO₂ substrates. The correlation between selectivity and reactant exposure serves to increase fundamental insights into the effects of sub-saturated self-limiting surface reactions on the quality and effectiveness of ASD processes and methods.

Published under license by AIP Publishing. <https://doi.org/10.1063/5.0013552>

18 July 2020 11:46:39

I. INTRODUCTION

Area-selective deposition (ASD) can provide alternative bottom-up options for atomic-scale material placement and nanoscale patterning, thereby complementing top-down lithography in semiconductor manufacturing.¹ Bottom-up ASD can aid in device miniaturization while enabling uniform deposition on complex 3D structures with atomic-scale precision.² Exploiting the observation that adsorption of certain deposition precursors depends strongly on the chemical termination present on the initial growth surface, noticeable growth can be achieved on a receptive surface while simultaneously limiting growth on adjacent non-receptive regions. As feature sizes shrink to <10 nm, physical alignment and over-lay of multiple features and line-edges become significant challenges. Chemical self-alignment has the potential to bypass the challenges in physical feature alignment, enabling new device designs and

manufacturing schemes.³ As such, the field of area-selective deposition is becoming increasingly vital for the continuation of Moore's law and viability of advanced device architectures.

Although in an ideal case no growth should be present on the non-receptive surface, the exposure of ALD precursors can modify surface termination, generating nucleation sites and subsequent undesired film growth.⁴ Area-selective deposition requires eliminating nucleation on the preferred non-growth regions, while maintaining good growth on the preferred growth regions. To combat the problem of unwanted nuclei, a common approach is to passivate the surface by forming patterns of organic molecules or monolayers to block growth on the covered areas.^{5–8} Another method that does not require organic molecule integration employs intermittent atomic layer etching (ALE) steps within the ALD cycle, i.e., ALD/ALE "super-cycles," to periodically remove unwanted nuclei from the non-growth substrate.⁹

Atomic layer deposition of metal oxides on Si-OH vs Si-H surfaces have been extensively researched related to high- κ dielectric scaling. A work by Puurunen compares the behavior of ALD of HfO₂ on varying density of surface hydroxyl groups using three mathematical models: by Alam and Green, by Puurunen, and by Ylilammi.^{10–13} The work shows that while the physical explanations vary, the growth per cycle (GPC) of ALD using HfCl₄/H₂O is strongly dependent on the –OH concentration on the surface. While 1.0 nm thick chemical SiO₂ exhibits characteristic linear growth, the H-terminated Si surface exhibits a “substrate-inhibited” growth. This trend has been demonstrated experimentally and shows that HfO₂ grown on Si-H are rougher and have poor electrical properties compared to HfO₂ deposited on Si-OH.^{14–17} It has also been shown that during HfO₂ ALD deposition, the initially H-terminated surface oxidizes, forming an interstitial layer, which promotes growth.^{17–20} This substrate-inhibited growth is dependent on the temperature and precursors used.^{19,21,22} Similar trends have been demonstrated for other metal oxides such as ZrO₂^{20,21,23–26} and TiO₂.^{27,28}

Previously, our group studied ALD/ALE and reported TiO₂ ASD on SiO₂ with minimal deposition on Si-H surfaces using the same approach used in this work.²⁹ In the ALD/ALE sequence, the ALD cycles were stopped after a small number of nuclei appeared on the Si-H surface, and ALE cycles were introduced to remove the unwanted material. Repeating the ALD/ALE sequence allowed the net film thickness to increase on the desired growth region while minimizing growth on the desired non-growth region. The self-limiting ALE process permits a balance with the ALD, so that etching of the film on the desired growth surface only minutely affects the final deposited thickness.³⁰ A significant advantage of this approach is that both processing steps are carried out in a single reactor system at fixed temperature and require minimal number of steps with no plasma exposure or necessary lift-off.³¹ Compared to more commonly used plasma-enhanced ALE, thermal ALE used in this work enables conformal etching of the material.³² A possible downside is that coupling the deposition and etching sequences increases the total process time. A previous study²⁹ did not examine the effect of reactant exposure on selectivity or perform *in situ* measurements, which are the key elements in this study.

In situ analysis techniques monitor sample properties without interrupting the process or exposing the surface to atmosphere, thereby avoiding sample contamination and simplifying data analysis.^{33–35} Performing sample characterization using *in situ* tools is imperative when studying nucleation mechanisms, where minute features on the surface can otherwise become masked or degraded by ambient exposure.^{36–38} In addition, critical nuclei can be created in a few cycles, making it difficult to accurately collect data without real-time measurements.³⁹ *In situ* ellipsometry has been used to study nucleation of Pt on Al₂O₃,⁴⁰ growth of ultrathin TiN films,⁴¹ nucleation and growth of TiN/Si and TiN/GaN heterostructures,⁴² Cu ASD on Pd vs SiO₂/SiN,⁴³ and many more processes.^{39,44–49} By probing a material’s optical and electro-optical response, film thickness can be measured on different substrates, effectively quantifying the selectivity. Moreover, measuring the film thickness change during the ASD process enables us to understand the mechanism behind selectivity loss and the impact of processing conditions on ASD.

While the effect of reactant exposure time during ALD processing is widely explored and well-understood,^{36,50–55} previous

reports of area-selective ALD generally use exposure conditions suitable for the desired deposition, without addressing how exposure and other process variables influence reactions on the non-growth surface. Mackus *et al.* demonstrated the impact of oxygen exposure on the nucleation of Pt during ALD and showed that longer O₂ dosing time increased the rate of Pt nucleation on an Al₂O₃ film surface.³⁶ Additionally, the influence of precursor pressure on area-selective deposition of Al₂O₃ on Ti has been previously studied using self-assembled monolayers (SAMs) as blocking layers and was shown that increasing precursor pressure led to lower selectivity due to increased physisorption on SAMs.⁵⁶

The work presented here explores the effect of ALD reactant dosing times during area-selective ALD of TiO₂ on Si-OH vs Si-H, which is an isothermal process in the sense that the reaction temperature is held constant throughout the experiment. The ALD/ALE sequence examined was described previously^{29,57} and provides a valuable model to understand ASD and the means to control the extent of selectivity. This work presents a systematic *in situ* study addressing the effects of ALD conditions on net ASD selectivity.

II. EXPERIMENTAL DETAILS

A. Reactor design

The ALD and ALE processes were carried out in a home-built warm-walled reaction chamber equipped with a four-wavelength ellipsometer (Film Sense FS-1) capable of *in situ* measurement of thin film optical properties. A simplified schematic of the reaction chamber is presented in Fig. 1. The sample is introduced to the chamber on a sample chuck, which locks onto a sample stage, heated by PID-controlled cartridge heaters and thermally isolated

18 July 2025 11:46:39

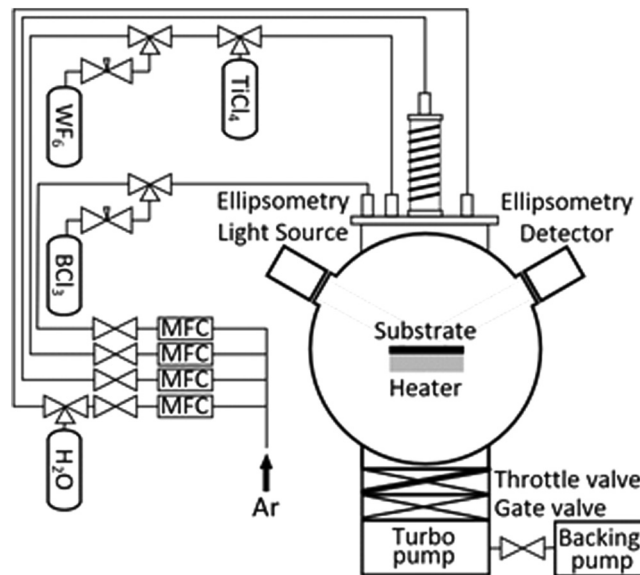


FIG. 1. Simplified schematic representation of deposition chamber used in this work, including the gas-delivery lines setup, pumping system, and attached spectroscopic ellipsometer.

from the rest of the chamber via ceramic standoffs. The substrate temperature can be controlled between 50 °C and 350 °C, while the reactor wall is typically 100 °C. Compared to isothermal hot-wall reactors, this differentially heated sample holder has the benefit of allowing the sample temperature to be adjusted relatively quickly.

The precursors are introduced to the system through four heated stainless-steel gas-delivery lines using argon (99.999% purity, Arc3 Gases) as a carrier and purge gas: line #1 hosted BCl_3 (99.9% purity, Matheson); line #2 TiCl_4 (99% purity, Strem Chemicals) and WF_6 (99.99% purity, Galaxy Chemical); line #3 de-ionized H_2O ; line #4 was only used for flowing argon. The argon flow rates were controlled by mass-flow controllers present on each line, and the precursors were dosed using pneumatic diaphragm valves (Swagelok, ALD series) controlled by a Python interface using automated process recipes. The gases and by-products are pumped out of the system using a Seiko-Seiki STP-300C turbo pump backed by an Alcatel 2021a two-stage rotary vane pump with activated aluminum and Sodasorb filters to shield the pump oil from harmful vapors. The pressure was controlled by a throttle valve located before the turbo pump and monitored by a Baratron capacitance manometer (0–10 Torr range, 0.1 mTorr resolution). During the Ar purge step, the throttle valve position produces a process pressure of 600 mTorr. Dosing leads to a small increase in process pressure due to the precursor partial pressure.

B. Substrate preparation

Two types of silicon wafer pieces were used as deposition substrates in this study: (1) boron-doped p-type silicon (100) wafers with 5–10 $\Omega \text{ cm}$ resistivity, blanket-terminated with either a chemical oxide or hydrogen; and (2) Si-H/ SiO_2 patterned wafers prepared by photolithographic wet etching of ~100 nm thick SiO_2 , resulting in alternating Si/ SiO_2 lines with 6 μm pitch (3 μm lines/spaces). The wet etching process produced a tapered edge on the SiO_2 features. Both the blanket and the patterned wafers were cleaved into $\sim 2 \times 2$ cm squares, submerged for 15 min in a piranha solution (1:1 mixture of $\text{H}_2\text{O}_2:\text{H}_2\text{SO}_4$) to remove organic residue and to form a hydroxyl-terminated (Si-OH) chemical oxide layer. To form a hydrogen-terminated (Si-H) substrate, the piranha-cleaned wafers were dipped into 5% HF solution for 30 s.

Immediately prior to loading samples into the reactor, they were rinsed with de-ionized water and blown dry with flowing nitrogen. They were then placed onto a sample chuck and secured in place using a physical clamp. The chamber was pumped down to $\sim 10^{-5}$ Torr, and the temperature and the pressure were allowed to stabilize for 30 min before any processing.

C. Deposition and etching process

Deposition and etching were carried out at 170 °C. The TiO_2 ALD sequence included discrete TiCl_4 and de-ionized water doses with argon as the purge and carrier gas. The dosing times for both precursors were varied from 90 ms to 270 ms. After every dose, the chamber was purged with argon for 20 s, followed by a 10 s pump down by completely opening the throttle valve to the turbo pump, evacuating the chamber to 10^{-5} Torr. After this pump step, the throttle valve was partially closed and the flow of argon resumed for 15 s to bring the system back to the operating pressure of

600 mTorr. This was followed by the subsequent H_2O or TiCl_4 dose step. The timing sequence is designated as $\text{TiCl}_4/\text{Ar}/\text{pump}/\text{Ar}/\text{H}_2\text{O}/\text{Ar}/\text{pump}/\text{Ar} = x/20/\text{pump}/15/x/20/\text{pump}/15$ s, where x ranges from 90 to 270 ms.

The atomic layer etching process coupled alternating WF_6 and BCl_3 doses. Based on earlier measurements and thermodynamic calculations⁵⁷ exposing TiO_2 to WF_6 at $T > 125$ °C fluorinates the TiO_2 surface, forming solid $\text{WO}_x\text{F}_y/\text{TiO}_y\text{F}_z$ and volatile TiF_4 . At $T < 190$ °C, subsequent BCl_3 exposure removes the W species and forms solid B_2O_3 . The boron oxide is then removed by the next WF_6 dose, thereby achieving self-limiting ALE.⁵⁷ The timing sequence during ALE follows $\text{WF}_6/\text{Ar}/\text{pump}/\text{Ar}/\text{BCl}_3/\text{Ar}/\text{pump}/\text{Ar} = 0.1/20/\text{pump}/15/0.1/20/\text{pump}/15$ s. Under these conditions, the rate of ALE was measured to be 0.11 nm/cycle under steady-etch conditions.

The ALD/ALE super-cycle sequence used here consists of 30 ALD cycles followed by 5 ALE cycles. The number of ALD/ALE cycles was selected based on successful results published previously.²⁹ This sequence was repeated N times (where $N = 10, 20,$ or 30) and is designated here as (30/5) $\times N$.

D. Process characterization

An *in situ* four-wavelength spectroscopic ellipsometer (Film Sense FS-1) directly attached to the chamber was used to monitor film thickness during the ALD/ALE sequence. The ellipsometer was positioned at a $65^\circ \pm 1^\circ$ incident angle and ellipsometry parameters Ψ and Δ were acquired at wavelengths 465 nm, 525 nm, 580 nm, and 635 nm. The ellipsometer was isolated from the chamber by two quartz windows and pneumatic gate valves that were opened and closed by electronic actuation in sequence with the process cycle. The gate valves were opened and ellipsometry data collected only during purge/pump periods, thereby preventing deposition on the windows. For this study, we collected ellipsometric data after every five ALD cycles and after every one ALE cycle. For the ALD step, data were collected after the water dose, and for ALE, data were collected after the BCl_3 step. Ellipsometry data collection required 9 s for full data collection. For blanket substrates, the TiO_2 film thickness was obtained from the ellipsometry data using a Cauchy model in the ellipsometer software, which takes into account the temperature-dependence of the optical response.

An example of raw ellipsometry data and the resulting thickness output are shown in Fig. 2. The values for Ψ , Δ , and thickness are shown for a single super-cycle of TiO_2 ASD on the Si-OH surface, consisting of 30 ALD cycles followed by 5 ALE cycles performed at 170 °C with 90 ms dosing times for both TiCl_4 and H_2O . While the value of Ψ does not change significantly in this thickness range, there is an evident correlation between the Δ and TiO_2 film thickness values. The Δ parameter characterizes the phase change upon reflection of the polarized light, which is highly sensitive to thickness changes in ultrathin layers.⁵⁸ While analyzing nucleation behavior using spectroscopic ellipsometry data, it is important not to over-interpret the thickness output by the model as it usually presumes a continuous thin film.⁵⁹

To compare selectivity for different materials or process approaches, the selectivity fraction, S , is defined as the difference between the surface coverage on growth surface, θ_1 , and that on the

18 July 2020 11:46:39

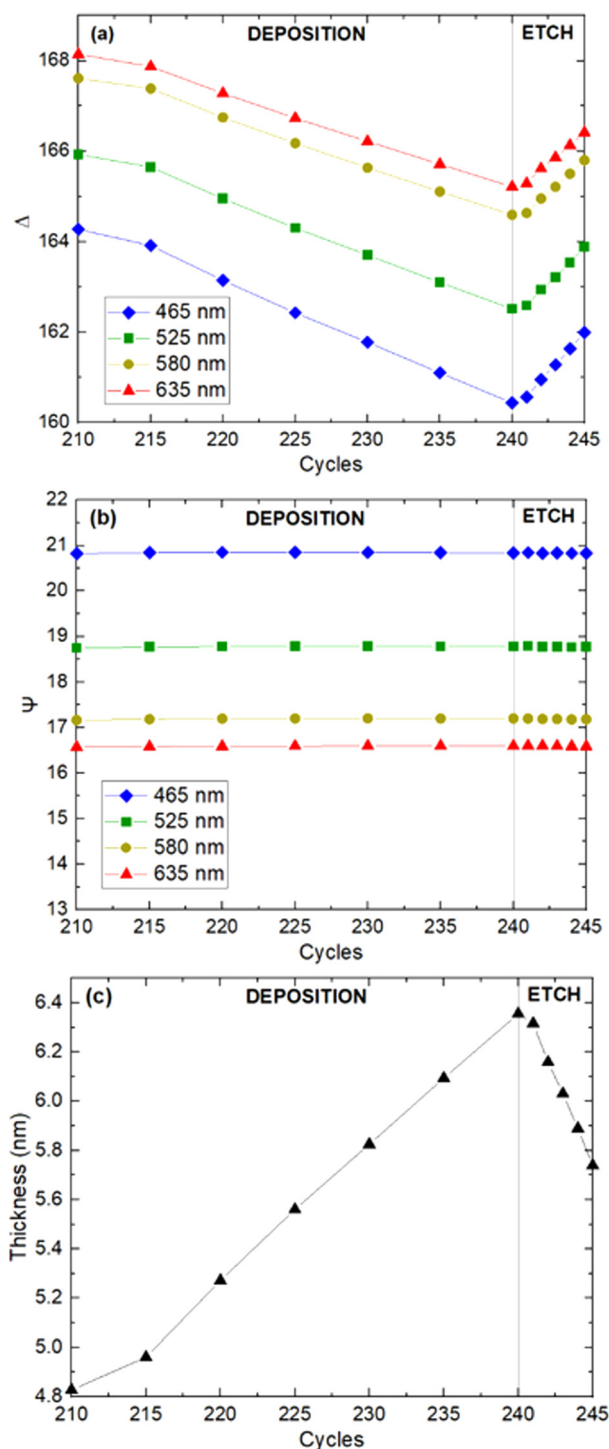


FIG. 2. *In situ* ellipsometry data collected during deposition and etching steps on the Si-OH surface. (a) and (b) show the raw Δ and Ψ parameters, respectively, which are fitted by a Cauchy model to (c) measure the TiO_2 layer thickness.

non-growth surface, θ_2 , relative to the total coverage on both surfaces.^{59–61} When the coverage on the non-growth surface is relatively small, a reasonable estimate for S is found using the measured film thicknesses on the growth and non-growth surfaces, t_1 and t_2 , respectively,

$$S = \frac{\theta_1 - \theta_2}{\theta_1 + \theta_2} \approx \frac{t_1 - t_2}{t_1 + t_2}. \quad (1)$$

When growth proceeds on the desired surface, and no growth appears on the non-growth surface, the process is perfectly selective and $S = 1$. When unwanted growth occurs on the non-growth region, S decreases, reaching 0 when both surfaces become fully covered. By setting a target S , which might be needed for practical ASD applications, one can determine from experimental measurements the threshold thickness that can be achieved on the growth surface before the value of S drops below target and selectivity loss occurs.

E. Material characterization

The chemical composition of blanket films on Si-OH and Si-H was determined by *ex situ* XPS using Kratos Axis Ultra DLD X-ray Photoelectron Spectrometer and the CasaXPS software package. The analysis consisted of survey scans followed by high-resolution scans for the elements Ti, Si, O, Cl, F, and C. The energy axes were calibrated using an adventitious carbon peak at 285.0 eV. Field emission scanning electron microscopy (FESEM Verios 460L), with a low energy electron detector operating at 10 kV and 0.8 nA was used to obtain the patterned Si/SiO₂ images. Focused ion beam (FIB, FEI Quanta 3D FEG instrument) with a high current Ga liquid metal ion gun was used for a TEM sample preparation. Cross-sectional images were obtained by scanning transmission electron microscopy (STEM, Jeol 2000FX) with energy dispersive spectrometer (EDS) attachment for chemical characterization of the patterned samples.

III. RESULTS AND DISCUSSION

A. Effect of dosing time on ALD growth

Figure 3 displays saturation curves obtained during steady ALD of TiO₂ at 170 °C, where the thickness growth per cycle (GPC) is plotted vs the dosing time of TiCl₄ or H₂O. The curves are obtained by fixing one of the precursor dosing times at 300 ms and varying the other between 0 and 300 ms. The thickness per cycle at each condition was measured after 50 deposition cycles, and the average value was plotted vs dosing time. Note that the shortest time used for open-dosing is 60 ms. This maximum value switching speed was limited by the computer interface communication rate. Figure 3(a) shows that for a fixed 300 ms H₂O dosing time, changing the TiCl₄ dosing time between 60 and 300 ms had minimal influence on the growth, with good saturation at ~0.05 nm/cycle. Similarly, Fig. 3(b) shows that fixing TiCl₄ dosing time at 300 ms and varying H₂O dosing time results in similar saturation at the same ~0.05 nm/cycle. Saturation requires ~100 ms of H₂O dosing time, whereas in Fig. 3(a), saturation is observed for the shortest 60 ms TiCl₄ dosing time.

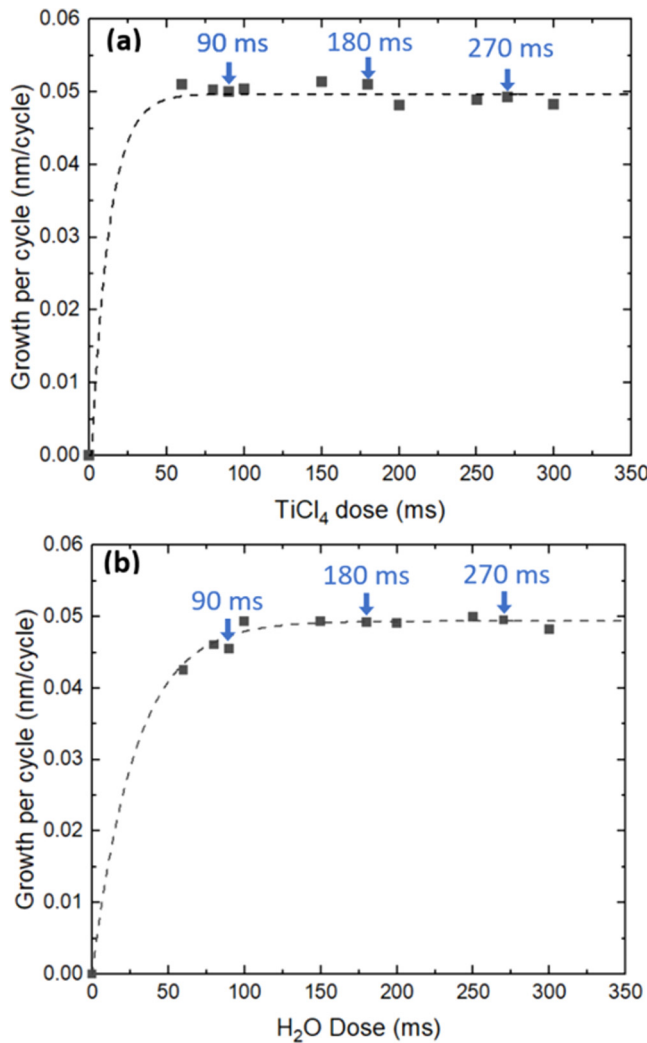


FIG. 3. Growth per cycle (GPC) of TiO₂ thin films deposited on Si-OH surface measured by *in situ* ellipsometry. One of the precursor dosing times is held constant at 300 ms, while the dosing time of (a) TiCl₄ and (b) H₂O is varied.

To study the effect of dosing conditions on nucleation on Si-H surfaces, growth was monitored under different dose conditions. As a first test, the TiCl₄ and H₂O dosing times were set equal to each other at 90 ms, 180 ms, or 270 ms, which can be referred to as “near-saturated,” “saturated,” and “oversaturated,” respectively, based on H₂O saturation levels. It is important to note that TiCl₄ dose reached saturation at all dosing times. A total of 150 TiO₂ ALD cycles were performed on freshly prepared Si-H surfaces, and deposition was monitored by *in situ* ellipsometry as a function of ALD cycle. For comparison, these three experiments were also repeated on Si-OH substrates. We note from the results shown in Fig. 3 that all three dosing conditions are close to or well within the saturated ALD regime. Therefore, the growth on each substrate type is expected to be nearly the same for each dose condition.

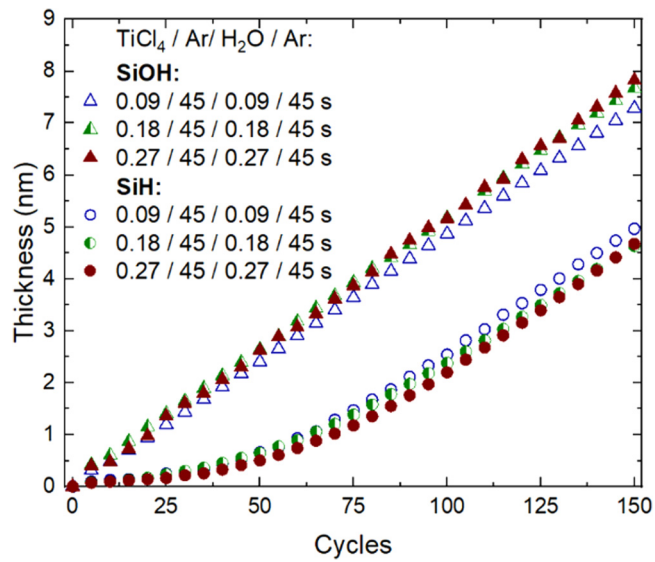


FIG. 4. The thickness of the TiO₂ layer on Si-OH and Si-H surfaces for 90 ms, 180 ms, and 270 ms TiCl₄/H₂O dosing times as measured by *in situ* ellipsometry.

The resulting six datasets (Si-OH and Si-H surfaces, three dosing conditions each) are shown in Fig. 4. On the Si-H substrates, all three dosing conditions show similar results, with noticeable growth delay up to ~25 ALD cycles, after which the GPC accelerates to near the steady value of ~0.05 nm/cycle. After 150 cycles, the thickness on all three Si-H surfaces is ~5 nm. The small differences in the growth rates reflect minute run-to-run variations on the surface. Likewise, on Si-OH, the different dose conditions show nearly identical results: 150 ALD cycles yielding ~8 nm of TiO₂ with the lowest dosing time condition resulting in the lowest film thickness as expected due to near-saturation condition. Using Eq. (1), the trend in film nucleation yields a film thickness of ~1.5 nm when selectivity S = 0.9 for all three conditions. These results indicate that near- and oversaturated H₂O dosing do not substantially affect the initial nucleation delay on the Si-H surface.

B. Combined ALD/ALE super-cycles

Next, we worked to understand how different saturated ALD dosing times could influence nucleation on the desired non-growth surface during more extended ASD conditions using ALD/ALE super-cycles. For this test, Si-H substrates were exposed to multiple ALD/ALE super-cycles, where the ALD dosing times per cycle were the same as those used to collect data in Fig. 4. The ALE cycles followed the conditions described in the experimental section. Figure 5 shows the resulting thickness values measured by *in situ* ellipsometry, plotted vs number of ALD/ALE super-cycles for all three deposition dose conditions. Note that on the plot, the data collected using 180 ms and 270 ms dosing times are offset on the y axis by 1 nm and 2 nm, respectively, to improve data visualization. Comparing results during the first three to five super-cycles, the

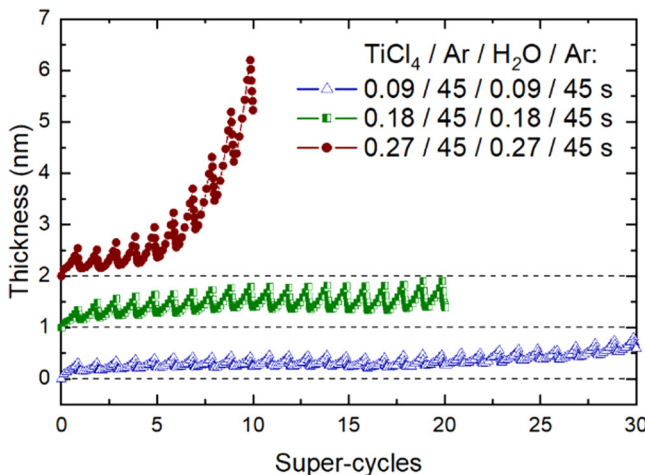


FIG. 5. The thickness of the TiO_2 layer on Si-H as a function of the number of super-cycles using $\text{TiCl}_4/\text{H}_2\text{O}$ dosing times of 90, 180, and 270 ms as measured by *in situ* ellipsometry. Data are collected after every five ALD cycles and after each individual ALE cycle. The data for 180 and 270 ms is offset on the y axis by 1 nm and 2 nm, respectively, to improve visualization.

different dosing times show similar trends in film deposition and etching. However, after ~ 5 super-cycles, for the 270 ms dosing time for both precursors, a significant amount of net deposition is present after ALE. As shown in Fig. 4, longer $\text{TiCl}_4/\text{H}_2\text{O}$ dose times (without ALE) did not influence the rate of unwanted nucleation on Si-H. However, in Fig. 5 where ALE cycles are used, longer $\text{TiCl}_4/\text{H}_2\text{O}$ dose times produced more rapid nucleation. This is ascribed to the removal of passivating Si-H bonds by the ALE etchant exposure, which allows more rapid formation Si-O sites that allow TiO_2 growth.²⁹ Interestingly, for all dosing conditions, the ellipsometry data indicate that during each sequence of five ALE steps, the amount of film removed per ALE cycle gradually

decreases, leaving a thin layer of “un-etched” film on the Si-H substrate. For example, for the case of 90 ms dosing times, ellipsometry indicates that after completing the etching for the 10th or 20th super-cycle, ~ 0.2 nm of TiO_2 remains on the Si-H surface. However, as discussed below, based on results from XPS analysis, the trend in ellipsometry is ascribed to the oxidation of the surface and formation of species not etched by the ALE process, rather than incomplete etching of TiO_2 .

XPS analysis was performed on Si-H samples exposed to various dosing conditions during ALD/ALE to evaluate the film deposition and chemical composition of the surface after the process was completed. The XPS data of the measured $\text{Ti} 2\text{p}$ signals on samples prepared with various dosing times are displayed in Fig. 6. All samples (including the starting Si-H) were measured by *ex situ* XPS, so differences in adventitious surface carbon and oxygen result from variations in ambient exposure for the different samples tested. However, there is an apparent trend of increasing O at. % as the dosing times and the number of super-cycles increase, which points to the oxidation of the non-growth region, promoting unwanted nucleation. Moreover, the starting Si-H and all other samples show mild fluorine contamination (> 0.2 at. %), which is ascribed to remanent fluorine from the HF-dip surface preparation before deposition. This premise is supported by the observation of clean hydrogen-terminated Si not exposed to ALD displaying F contamination of 3.1 at. %.

After 20 super-cycles using 90 ms TiCl_4 and H_2O dosing times [Fig. 6(a)], the XPS $\text{Ti} 2\text{p}$ spectrum shows no detectable signal. Considering that TiO_2 sensitivity on Si is about 0.3 at. %, the lack of measurable signal indicates that the maximum possible thickness of TiO_2 on that surface is ~ 0.04 nm, or $\sim 80\%$ of one monolayer,⁶² which is substantially less than suggested by the ellipsometry results in Fig. 5. Other XPS analysis (shown below) indicates that the WF_6 and BCl_3 used for ALE modify the surface and change the surface reflectivity, which the ellipsometry model interprets as the thickness increases.

The atomic percentages calculated from the elemental XPS peaks collected on the Si-H surface after ALD/ALE using the

18 July 2020 / 114639

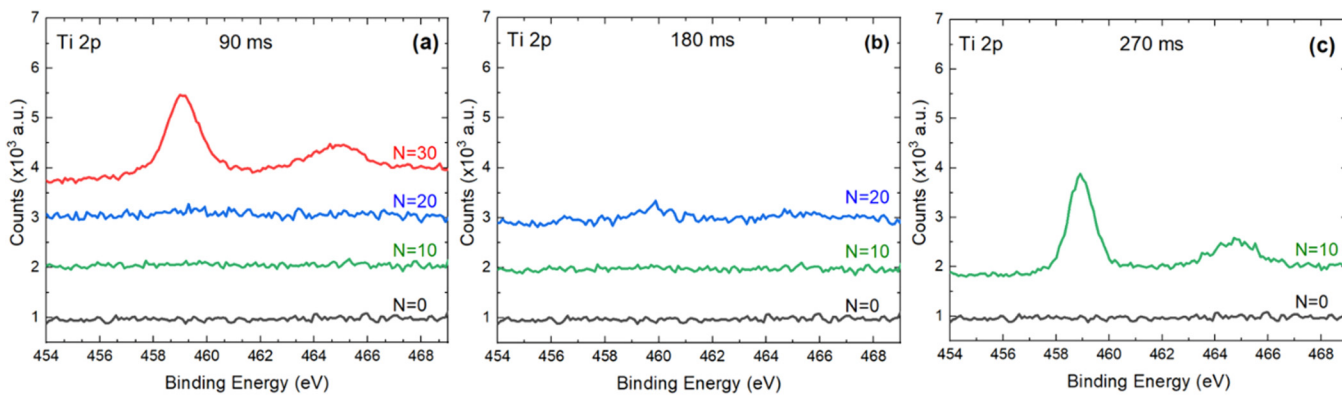


FIG. 6. XPS data of the $\text{Ti} 2\text{p}$ signal for deposition carried out using (a) 90, (b) 180, and (c) 270 ms H_2O and TiCl_4 dosing times for varying number of deposition/etch super-cycles (N) on Si-H.

TABLE I. Elemental composition of hydrogen-terminated (100) Si wafers exposed to different $\text{TiCl}_4/\text{H}_2\text{O}$ dosing times as measured by x-ray photoelectron spectroscopy (XPS). One super-cycle consists of 30 ALD and 5 ALE cycles.

Dosing time (ms)	Super-cycles	Ti (at. %)	Si (at. %)	O (at. %)	C (at. %)	B (at. %)	W (at. %)	F (at. %)	Cl (at. %)
0	0	0	72.7	9.0	15.2	0	0	3.1	0
90	10	0	72.9	17.2	8.7	0	0	1.2	0
	20	0	70.1	20.7	7.8	0	0	0.5	0.9
	30	1.2	64.1	20.2	10.3	0.1	0	4.1	0
180	10	0	65.4	21.4	12.0	0.1	0.1	0.4	0.7
	20	0.3	58.0	24.9	15.1	0.1	0.2	0.5	0.9
	270	4.5	43.9	30.1	17.6	0.2	0.2	2.7	0.8

different exposure times are summarized in Table I. With XPS data measured after every 10 super-cycles, the 270 ms dosing condition first exhibited the Ti 2p signal at 10 super-cycles (4.5 at. %); the 180 ms at 20 (0.3 at. %); and the 90 ms at 30 (1.2 at. %). This indicates that shorter dosing times help inhibit unwanted nucleation in the combined ALD/ALE process.

The spectra of measured B 1s and W 4d peaks are shown in Fig. S1 in the [supplementary material](#). As seen in Figs. S1(a)–S1(c) in the [supplementary material](#), the exact determination of B 1s signal is complicated due to overlapping Si 2s plasmon loss peak and low concentration of boron. However, the results indicate that only minor amounts of W and B contamination were detected (≤ 0.2 at. %) for higher dosing times.

To further distinguish the effect of TiCl_4 and H_2O dose amount on TiO_2 selectivity, the TiCl_4 and H_2O dosing times were varied independently, and Fig. 7 shows the resulting *in situ*

ellipsometry data collected during ALD/ALE on Si-H. This experiment consisted of two runs, one using $\text{TiCl}_4/\text{H}_2\text{O}$ dosing times of 270/90 ms and the other using 90/270 ms. The conditions were otherwise identical to those used for collecting data in Fig. 5, and data were collected for a total of 15 ALD/ALE super-cycles. The two datasets are clearly distinguishable with the larger H_2O dosing time condition displaying less nucleation delay than the shorter H_2O dosing time condition. Moreover, the shorter H_2O dose condition sample etches to a relatively constant optical thickness of 0.15–0.3 nm after each super-cycle. In comparison, the higher H_2O dosing time condition is unable to etch back to the initial baseline of the optical thickness after the sixth super-cycle, where the thickness after each super-cycle exceeds the previous. At the end of the 15 super-cycles, the 90/270 ms case resulted in a final thickness of ~ 1.2 nm, while the 270/90 ms $\text{TiCl}_4/\text{H}_2\text{O}$ case had a final thickness of ~ 0.4 nm. This noticeable difference between two conditions confirms that H_2O is the major factor in shortening the nucleation delay during ALD/ALE super-cycles on the Si-H surfaces. This effect of H_2O exposure is ascribed to oxidation of the initial

18 July 2020 11:46:39

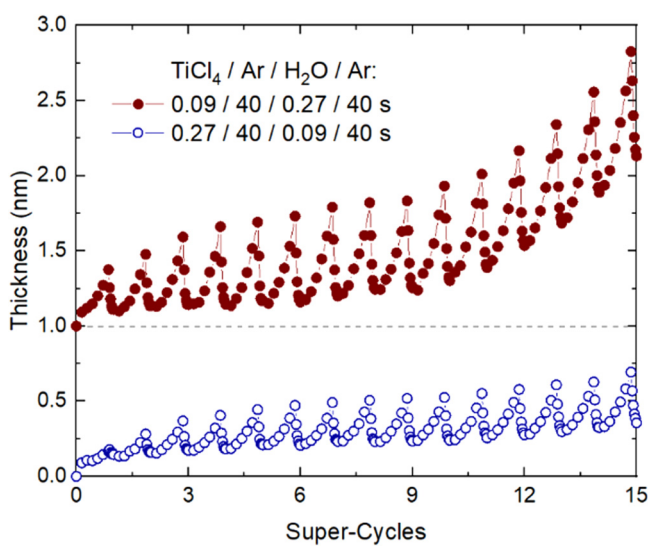


FIG. 7. The thickness of the TiO_2 layer on Si-H for $\text{TiCl}_4/\text{H}_2\text{O}$ 90/270 ms and 270/90 ms dosing times as measured by *in situ* ellipsometry. Data are shown for 15 super-cycles, consisting of 30 ALD and 5 ALE cycles each, with data points taken every five cycles for ALD and every cycle for ALE. The data for 90/270 ms are offset on the y axis by 1 nm to improve visualization.

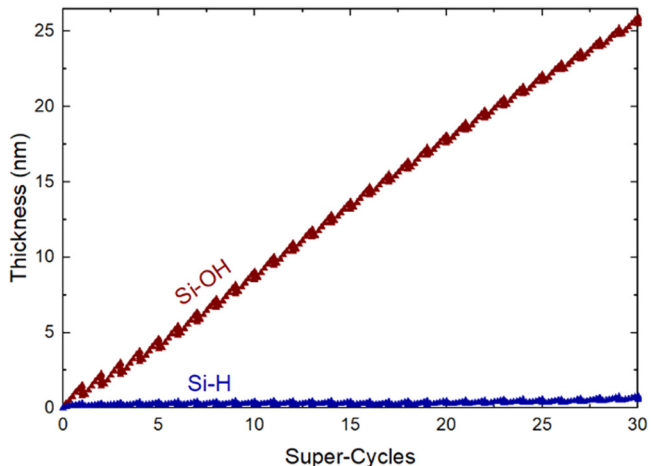


FIG. 8. TiO_2 film thickness on Si-H and Si-OH surfaces during ALD/ALE super-cycles with 90 ms dosing conditions for $\text{TiCl}_4/\text{H}_2\text{O}$. The measurement was done by *in situ* ellipsometry, with the data point taken after every five cycles for ALD and every cycle for ALE.

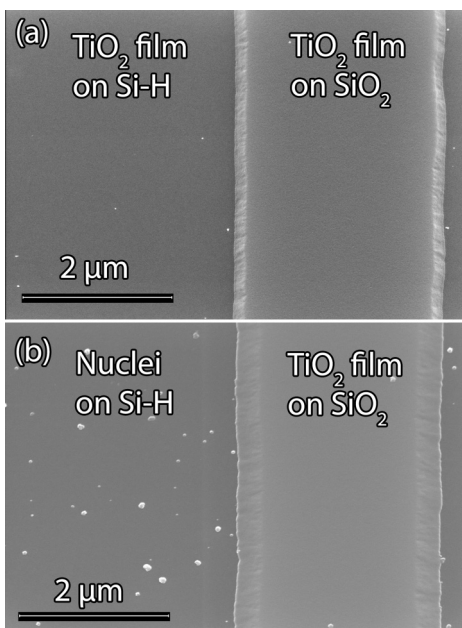


FIG. 9. SEM images of TiO_2 ALD/ALE on patterned Si/SiO_2 substrates using (a) 270 ms dosing conditions for 10 super-cycles and (b) 90 ms dosing conditions for 30 super-cycles.

hydrogen-terminated surface, promoting growth of mixed Ti/Si oxide. The ALE sequence used here is favorable for etching TiO_2 but not for etching SiO_2 .²⁹

Based on results in Figs. 6 and 7, the conditions using the shortest reactant exposure time are expected to produce the largest selectivity values. Figure 8 shows results obtained by *in situ* ellipsometry for 90 ms dosing times for the 30/5 ALD/ALE condition at 170 °C for 30 super-cycles measured during two identical runs, where the ellipsometer was focused on $\text{Si}-\text{OH}$ and $\text{Si}-\text{H}$, respectively. The final thicknesses were ~ 25.5 nm on the $\text{Si}-\text{OH}$ surface and ~ 0.6 nm on the $\text{Si}-\text{H}$ surface. Calculating the selectivity defined by Eq. (1) results in $S \approx 0.95$ for a thickness of 25.5 nm on the preferred growth surface. Extrapolation of the data using a model to quantify and predict nucleation indicates a selectivity of $S > 0.9$ up to 36.9 nm film thickness—a significant improvement from our previously reported result of 15 nm ASD for $S > 0.9$ using fully saturated dosing conditions,^{29,59} and even more notable compared to the ALD-only case, where $S > 0.9$ was limited to only 1.5 nm.

C. Effect of dosing time on patterned substrates

The effect of reactant dosing duration on the deposition of TiO_2 on Si/SiO_2 patterned substrates was studied using SEM. Figure 9 exhibits patterns exposed to 270/270 ms dosing conditions for 10 super-cycles and to 90/90 ms dosing conditions for 30 super-cycles. The growth conditions are the same as used to collect data

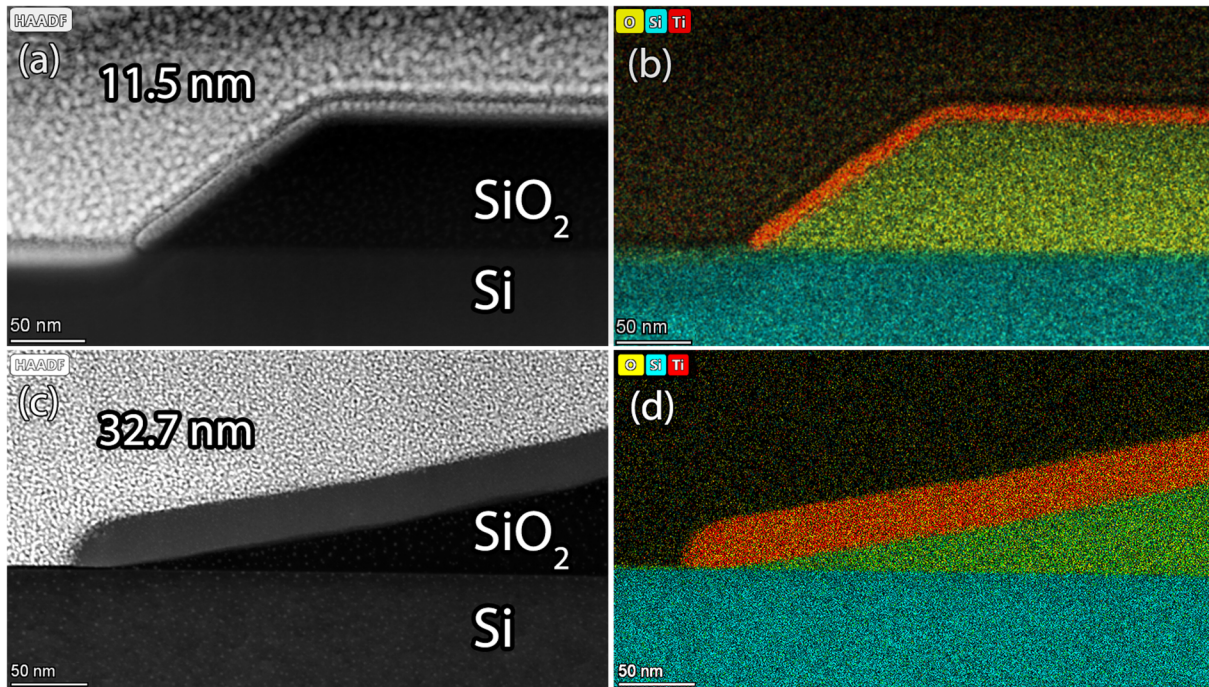


FIG. 10. (a) Cross-sectional TEM and (b) TEM-EDS mapping of 10 ALD/ALE super-cycles at 270 ms dosing conditions on Si/SiO_2 pattern. (c) Cross-sectional TEM and (d) TEM-EDS mapping of 30 ALD/ALE super-cycles at 90 ms dosing conditions on Si/SiO_2 pattern.

18 July 2020 11:46:39

shown in Fig. 5. The smooth surfaces observed using oversaturated dosing times [Fig. 9(a)] is consistent with blanket TiO₂ on both Si-H and SiO₂ surfaces. However, using near-saturated exposure times [Fig. 9(b)], a smooth blanket layer appears only on the SiO₂ surface, with less growth, appearing as visible isolated nuclei, on the Si-H surface.

To further study the effect of the reactant doses on promoting deposition on the non-growth surface, cross-sectional STEM images were taken of the Si/SiO₂ patterned substrates exposed to different dosing time conditions, and resulting images are presented in Fig. 10. The EDS analysis of samples deposited using 90/90 ms dosing times for 30 super-cycles and 270/270 ms dosing times for 10 super-cycles show no visible TiO₂ growth on the Si-H for either sample. However, a thin top layer of the initially hydrogen-terminated surface appears to have oxidized as indicated by a thin green layer visible in TEM-EDS images. As no detectable TiO₂ has deposited on top of this oxidized layer, it can be presumed to have oxidized during the preparation of the TEM cross section. Meanwhile, noticeable TiO₂ growth is present on the SiO₂ surface with measured film thickness of 11.5 nm for the 270/270 ms condition and 32.7 nm for the 90/90 ms condition. Although more detailed higher-resolution images are needed, it appears that the thicker TiO₂ film leads to “mushroom” growth, where the TiO₂ deposits from all directions on SiO₂, including laterally on the Si-H surface near Si/SiO₂ interface.

IV. CONCLUSION

The effect of reactant exposure on the selectivity of area-selective TiO₂ deposition has been investigated in a combined isothermal ALD/ALE process. *In situ* ellipsometry results show that extending the reactant exposure times during ALD maintains nearly the same growth per cycle on both Si-H and Si-OH surfaces. In contrast, overdosing TiCl₄/H₂O during ALD/ALE super-cycles leads to excess thickness increase on the preferred non-growth Si-H surface. Near-saturated H₂O dosing was shown to maintain a selectivity of $S \approx 0.95$ up to a TiO₂ film thickness of 25.5 nm on the Si-OH surface; a significant improvement from the ALD-only case, which resulted in a film thickness of 1.5 nm at $S \approx 0.9$.

Independently comparing TiCl₄ and H₂O dosing times, water was found to be the main cause for the selectivity loss, with longer H₂O dosing times exhibiting notably faster nucleation on Si-H. This loss of selectivity can be attributed to two main factors: (1) overexposure of the reactants leads to increased chance of interactions with the surface, prompting physisorption, and generation of potential nucleation sites; and (2) water vapor reacts with the exposed surface sites formed during ALE by the removal of Si-H bonds causing the growth of surface oxide species that are not etched by the TiO₂ ALE chemistry.

The mechanisms shown here for ASD using combined ALD/ALE steps indicate that selectivity loss is associated with alternate unfavorable reactions on the non-growth surface during extended ALD reactant exposures. Therefore, this work expands the understanding of effects of reactant exposure during area-selective ALD, where overexposure of one or both of the precursors may have a negligible effect during typical ALD, but leads to selectivity loss

during area-selective deposition. Although not studied explicitly in this work, adjusting the reactant dose times to improve selectivity could negatively impact the conformality of a desired film coating, for example, in high aspect ratio trenches where relatively long dose times are needed to achieve uniform deposition. As shown here, increasing the exposure beyond near-saturation can have a negative impact on overall deposition selectivity. We believe that achieving conformal deposition while maintaining high selectivity is an important challenge, which needs to be addressed in future works. In general, the effect of dosing duration on film nucleation helps further improve area-selective deposition and the ability to manipulate or minimize unwanted nucleation in future processes.

SUPPLEMENTARY MATERIAL

See the [supplementary material](#) for XPS data of B 1s and W 4d peaks for various process conditions.

ACKNOWLEDGMENTS

This material is based on the work supported by the National Science Foundation under Grant No. 1704151 and the Semiconductor Research Corporation (Task No. 2729.001). This work was performed in part at the Analytical Instrumentation Facility (AIF) at North Carolina State University, which is supported by the State of North Carolina and the National Science Foundation (Award No. ECCS-1542015). The AIF is a member of the North Carolina Research Triangle Nanotechnology Network (RTNN), a site in the National Nanotechnology Coordinated Infrastructure (NNCI). Some work was also performed in part at the Shared Materials Instrumentation Facility (SMIF) at Duke University. The authors thank S. Smith for the STEM characterization.

DATA AVAILABILITY

The data that support the findings of this study are available from the corresponding author upon reasonable request.

REFERENCES

- ¹N. Biyikli, A. Haider, P. Deminskyi, and M. Yilmaz, *Proc. SPIE* **10349**, 10349M (2017).
- ²A. J. M. Mackus, M. J. M. Merkx, and W. M. M. Kessels, *Chem. Mater.* **31**, 2 (2019).
- ³A. J. M. Mackus, A. A. Bol, and W. M. M. Kessels, *Nanoscale* **6**, 10941 (2014).
- ⁴R. Vallat, R. Gassiloud, B. Eychenne, and C. Vallée, *J. Vac. Sci. Technol. A* **35**, 1 (2017).
- ⁵F. S. Minaye Hashemi, B. R. Birchansky, and S. F. Bent, *ACS Appl. Mater. Interfaces* **8**, 33264 (2016).
- ⁶E. K. Seo, J. W. Lee, H. M. Sung-Suh, and M. M. Sung, *Chem. Mater.* **16**, 1878 (2004).
- ⁷J. R. Avila, E. J. Demarco, J. D. Emery, O. K. Farha, M. J. Pellin, J. T. Hupp, and A. B. F. Martinson, *ACS Appl. Mater. Interfaces* **6**, 11891 (2014).
- ⁸R. Chen, H. Kim, P. C. McIntyre, and S. F. Bent, *Chem. Mater.* **17**, 536 (2005).
- ⁹K. J. Kanarik, T. Lill, E. A. Hudson, S. Sriraman, S. Tan, J. Marks, V. Vahedi, and R. A. Gottscho, *J. Vac. Sci. Technol. A* **33**, 020802 (2015).
- ¹⁰R. L. Puurunen, *J. Appl. Phys.* **95**, 4777 (2004).
- ¹¹M. A. Alam and M. L. Green, *J. Appl. Phys.* **94**, 3403 (2003).
- ¹²R. L. Puurunen, *Chem. Vap. Deposition* **9**, 249 (2003).
- ¹³M. Yilammi, *Thin Solid Films* **279**, 124 (1996).

18 July 2020 11:46:39

- ¹⁴M. L. Green, M.-Y. Ho, B. Busch, G. D. Wilk, T. Sorsch, T. Conard, B. Brijs, W. Vandervorst, P. I. Räisänen, D. Muller, M. Bude, and J. Grazul, *J. Appl. Phys.* **92**, 7168 (2002).
- ¹⁵M. L. Green, A. J. Allen, X. Li, J. Wang, J. Ilavsky, A. Delabie, R. L. Puurunen, and B. Brijs, *Appl. Phys. Lett.* **88**, 032907 (2006).
- ¹⁶E. P. Gusev, C. Cabral, M. Copel, C. D'Emic, and M. Gribelyuk, *Microelectron. Eng.* **69**, 145 (2003).
- ¹⁷J.-F. Damlecourt, O. Renault, D. Samour, A.-M. Papon, C. Leroux, F. Martin, S. Marthon, M.-N. Sémeria, and X. Garros, *Solid State Electron.* **47**, 1613 (2003).
- ¹⁸J. C. Hackley, T. Gougousi, and J. D. Demaree, *J. Appl. Phys.* **102**, 034101 (2007).
- ¹⁹M. Cho, J. Park, H. B. Park, C. S. Hwang, J. Jeong, and K. S. Hyun, *Appl. Phys. Lett.* **81**, 334 (2002).
- ²⁰E. P. Gusev, E. Cartier, D. A. Buchanan, M. Gribelyuk, M. Copel, H. Okorn-Schmidt, and C. D'Emic, *Microelectron. Eng.* **59**, 341 (2001).
- ²¹P. D. Kirsch, M. A. Quevedo-Lopez, H.-J. Li, Y. Senzaki, J. J. Peterson, S. C. Song, S. A. Krishnan, N. Moumen, J. Barnett, G. Bersuker, P. Y. Hung, B. H. Lee, T. Lafford, Q. Wang, D. Gay, and J. G. Ekerdt, *J. Appl. Phys.* **99**, 023508 (2006).
- ²²J. Aarik, A. Aidla, A. Kikas, T. Käämbre, R. Rammula, P. Ritslaid, T. Uustare, and V. Sammelselg, *Appl. Surf. Sci.* **230**, 292 (2004).
- ²³M. Copel, M. Gribelyuk, and E. Gusev, *Appl. Phys. Lett.* **76**, 436 (2000).
- ²⁴S. Ferrari, M. Modreanu, G. Scarel, and M. Fanciulli, *Thin Solid Films* **450**, 124 (2004).
- ²⁵R. L. Puurunen, W. Vandervorst, W. F. A. Besling, O. Richard, H. Bender, T. Conard, C. Zhao, A. Delabie, M. Caymax, S. De Gendt, M. Heyns, M. M. Viitanen, M. de Ridder, H. H. Brongersma, Y. Tamminga, T. Dao, T. de Win, M. Verheijen, M. Kaiser, and M. Tuominen, *J. Appl. Phys.* **96**, 4878 (2004).
- ²⁶K. Kukli, M. Ritala, J. Aarik, T. Uustare, and M. Leskelä, *J. Appl. Phys.* **92**, 1833 (2002).
- ²⁷R. Methaapanon and S. F. Bent, *J. Phys. Chem. C* **114**, 10498 (2010).
- ²⁸D. R. G. Mitchell, D. J. Attard, and G. Triani, *Thin Solid Films* **441**, 85 (2003).
- ²⁹S. K. Song, H. Saare, and G. N. Parsons, *Chem. Mater.* **31**, 4793 (2019).
- ³⁰K. J. Kanarik, S. Tan, and R. A. Gottscho, *J. Phys. Chem. Lett.* **9**, 4814 (2018).
- ³¹S. M. George and Y. Lee, *ACS Nano* **10**, 4889 (2016).
- ³²C. Fang, Y. Cao, D. Wu, and A. Li, *Prog. Nat. Sci. Mater. Int.* **28**, 667 (2018).
- ³³E. Langereis, S. B. S. Heil, H. C. M. Knoops, W. Keuning, M. C. M. van de Sanden, and W. M. M. Kessels, *J. Phys. D Appl. Phys.* **42**, 073001 (2009).
- ³⁴M. T. Kief, *Proc. SPIE* **10294**, 1024903 (1999).
- ³⁵M. Junige, M. Geidel, M. Knaut, M. Albert, and J. W. Bartha, in *IEEE Semiconductor Conference Dresden, Dresden* (IEEE, 2011).
- ³⁶A. J. M. Mackus, M. A. Verheijen, N. Leick, A. A. Bol, and W. M. M. Kessels, *Chem. Mater.* **25**, 1905 (2013).
- ³⁷T. Muneshwar and K. Cadien, *Appl. Surf. Sci.* **328**, 344 (2015).
- ³⁸R. W. Wind, F. H. Fabreguette, Z. A. Sechrist, and S. M. George, *J. Appl. Phys.* **105**, 074309 (2009).
- ³⁹L. Lecordier, S. Herregods, and S. Armini, *J. Vac. Sci. Technol. A* **36**, 031605 (2018).
- ⁴⁰L. Baker, A. S. Cavanagh, D. Seghete, S. M. George, A. J. M. MacKus, W. M. M. Kessels, Z. Y. Liu, and F. T. Wagner, *J. Appl. Phys.* **109**, 084333 (2011).
- ⁴¹E. Langereis, S. B. S. Heil, M. C. M. Van De Sanden, and W. M. M. Kessels, *J. Appl. Phys.* **100**, 023534 (2006).
- ⁴²P. Patsalas and S. Logothetidis, *J. Appl. Phys.* **93**, 989 (2003).
- ⁴³X. Jiang, H. Wang, J. Qi, and B. G. Willis, *J. Vac. Sci. Technol. A* **32**, 041513 (2014).
- ⁴⁴M. Junige, M. Löfller, M. Geidel, M. Albert, J. W. Bartha, E. Zschech, B. Rellinghaus, and W. F. van Dorp, *Nanotechnology* **28**, 395301 (2017).
- ⁴⁵M. A. Raza, H. J. W. Zandvliet, B. Poelsema, and E. S. Kooij, *J. Appl. Phys.* **113**, 233510 (2013).
- ⁴⁶M. F. J. Vos, S. N. Chopra, M. A. Verheijen, J. G. Ekerdt, S. Agarwal, W. M. M. Kessels, and A. J. M. Mackus, *Chem. Mater.* **31**, 3878 (2019).
- ⁴⁷V. Pesce, C. Vallee, R. Gassilloud, A. Chacker, M. Bonvalot, B. Pelissier, N. Posseme, and A. Bsisy, in *AVS 65th International Symposium* (AVS, 2018).
- ⁴⁸A. Mameli, M. J. M. Merkx, B. Karasulu, F. Roozeboom, W. M. M. Kessels, and A. J. M. Mackus, *ACS Nano* **11**, 9303 (2017).
- ⁴⁹A. Mameli, B. Karasulu, M. A. Verheijen, B. Barcones, B. Macco, A. J. M. Mackus, W. M. M. E. Kessels, and F. Roozeboom, *Chem. Mater.* **31**, 1250 (2019).
- ⁵⁰K. M. Niang, G. Bai, and J. Robertson, *J. Vac. Sci. Technol. A* **38**, 042401 (2020).
- ⁵¹Z. Baji, Z. Lábádi, Z. E. Horváth, G. Molnár, J. Volk, I. Bársóny, and P. Barna, *Cryst. Growth Des.* **12**, 5615 (2012).
- ⁵²R. Kuse, M. Kundu, T. Yasuda, N. Miyata, and A. Toriumi, *J. Appl. Phys.* **94**, 6411 (2003).
- ⁵³C. A. Murray, S. D. Elliott, D. Hausmann, J. Henri, and A. LaVoie, *ACS Appl. Mater. Interfaces* **6**, 10534 (2014).
- ⁵⁴K. Kukli, J. Aarik, M. Ritala, T. Uustare, T. Sajavaara, J. Lu, J. Sundqvist, A. Aidla, L. Pung, A. Härsta, and M. Leskelä, *J. Appl. Phys.* **96**, 5298 (2004).
- ⁵⁵R. G. Gordon, D. Hausmann, E. Kim, and J. Shepard, *Chem. Vap. Deposition* **9**, 73 (2003).
- ⁵⁶S. Seo, B. C. Yeo, S. S. Han, C. M. Yoon, J. Y. Yang, J. Yoon, C. Yoo, H.-J. Kim, Y.-B. Lee, S. J. Lee, J.-M. Myoung, H.-B.-R. Lee, W.-H. Kim, I.-K. Oh, and H. Kim, *ACS Appl. Mater. Interfaces* **9**, 41607 (2017).
- ⁵⁷P. C. Lemaire and G. N. Parsons, *Chem. Mater.* **29**, 6653 (2017).
- ⁵⁸E. Garcia-Caurel, A. De Martino, J. P. Gaston, and L. Yan, *Appl. Spectrosc.* **67**, 1 (2013).
- ⁵⁹G. N. Parsons, *J. Vac. Sci. Technol. A* **37**, 020911 (2019).
- ⁶⁰W. L. Gladfelter, *Chem. Mater.* **5**, 1372 (1993).
- ⁶¹G. N. Parsons and R. D. Clark, *Chem. Mater.* **32**, 4920 (2020).
- ⁶²A. G. Shard, *Surf. Interface Anal.* **46**, 175 (2014).